# *IN VIVO* DIFFUSE OPTICAL SPECTROSCOPY AND IMAGING OF BLOOD DYNAMICS IN BRAIN

A. G. YODH, C. CHEUNG, J. P. CULVER, AND T. DURDURAN

*Department of Physics and Astronomy, University of Pennsylvania, Philadelphia, PA 19104-6396, USA*

*E-mail: yodh@physics.upenn.edu*

J. H. GREENBERG, K. TAKAHASHI, AND D. FURUYA

*Department of Neurology, University of Pennsylvania, Philadelphia, PA 19104, USA*

In this paper we provide a cursory review on diffuse optical probes and their relevance to the investigation of human tissues. Then we describe a recent instrument we have built and used to study variations of blood flow, hemoglobin concentration, and blood oxygen saturation in the functioning rat brain. The instrument combines two novel optical methodologies. Diffuse correlation spectroscopy monitors changes in the cerebral blood flow by measuring the optical phase-shifts caused by moving blood cells. Diffuse near-infrared absorption spectroscopy concurrently measures tissue absorption at two wavelengths to determine hemoglobin concentration and blood oxygen saturation in the same tissue volume. The optical probe is non-invasive and was employed through the intact skull. The utility of the technique is demonstrated *in vivo* by measuring the temporal changes in the regional vascular dynamics of rat brain during hypercapnia and hypoxia.

## 1 Introduction

Light spectroscopies are particularly well suited for the study of simple, homogenous, optically thin samples. Unfortunately many practical materials are not so simple. Human tissues, for example, are highly scattering media. Light penetration in tissues is limited, and the effects of tissue absorption and internal motion must be separated from the effects of tissue scattering. Nevertheless, the use of light to investigate the human body interior has grown enormously in recent years, in part as a result in advances in our fundamental understanding about light transport in highly scattering materials, and in part as a result of technological innovations in optics [1].

The application of near-infrared (NIR) optical methods for tissue characterization is attractive for several reasons. The techniques utilize non-ionizing radiation, are non-invasive, and are often technologically simple and fast. These features have lead to compact, portable, and inexpensive clinical instruments in medicine, e.g. the pulse oximeter. The optical method also has several unique measurable parameters. Blood dynamics, blood volume, blood oxygen saturation, and water content of a rapidly growing tumor are often substantially different than normal tissue, and will





alter tissue optical absorption coefficients. An increase in organelle population (e.g. mitochondria) often accompanies the higher metabolic activity of rapidly growing tissues, and leads to an increased scattering coefficient. Similarly the optical absorption, fluorescence, and scattering of exogenous contrast agents such as Indocyanine green (ICG) that occupy vascular and extravascular space provide useful forms of sensitization.

Arguably the most critical advance in the field has been the recognition and widespread acceptance that light transport over long distances in tissues is well approximated as a diffusive process. Using this physical model it is possible to quantitatively separate tissue scattering from tissue absorption, and to accurately incorporate the influence of boundaries, such as the air-tissue interface, into the transport theory. Waves of diffuse light energy density or their time-domain analogs propagate deeply in tissues (i.e. ~10 cm) and exhibit simple "optical" phenomena such as refraction, diffraction, interference, and dispersion as they encounter variations in tissue optical properties [2–6]. The diffusion approximation is also critical because it provides a tractable basis for tomographic approaches to image reconstruction of tissue optical properties using highly scattered light [7–14].

Physiological applications of diffuse light imaging and spectroscopy include functional imaging and detection of brain bleeds, quantitation of brain physiology and function, study of mitochondrial diseases, study of muscle function and physiology, optical mammography, optical dosimetry in photodynamic therapy of cancer, and early detection of cancer. This paper focuses on some recent advances made in our lab to monitor oxygen metabolism in rat brain [15].

The vascular changes that accompany neuronal activity represent a critical and incompletely understood component of neurophysiology. Energy is required for cerebral functions, and its conversion into a useful form is facilitated by oxygen delivered to the brain through the cerebral vasculature. A range of non-invasive techniques have been used to probe activation of the cerebral cortex. Electrical signals originating from the firing of neurons can be measured with electroencephalography (EEG), changes in local cerebral glucose utilization and local cerebral blood flow can be measured with positron emission tomography (PET) [16], and changes in the concentration of deoxyhemoglobin and adenosine triphosphate can be measured with magnetic resonance imaging (MRI) [17,18]. Some relatively more invasive methods for studying the brain include laser Doppler flowmetry (LDF) and confocal microscopy. Both of these methods are used to study near-surface (or nearprobe) tissue volumes. LDF measures the blood flow speed and the number of moving blood cells [19]. However, LDF is primarily a surface technique, and in order to make these measurements in brain tissue the skull must be thinned to achieve sufficient signal. Confocal microscopy has been used to image

the cortical capillary bed and erythrocytes through a cranial window. In this case, blood flow is estimated by counting the number of blood cells flowing through a capillary per unit time [20]. Finally, a number of other techniques have been applied to measure cerebral tissue oxygen. These include microelectrodes [21], phosphorescence quenching by oxygen in the microvasculature [22], and near-infrared spectroscopy (NIRS). NIRS relies on the difference between the absorption spectra of oxyhemoglobin and deoxyhemoglobin to determine blood oxygenation [23]. Generally these methods provide complementary information about brain tissue, and no technique has emerged as a universal choice for experiments in neurophysiology.

In our study we combine diffuse photon correlation methods, originally used to investigate highly scattering complex fluids [24–26], with a near-infrared diffuse wave regional imager [23] for hemoglobin spectroscopy. The instrument enables us to simultaneously measure regional blood perfusion, hemoglobin concentration and blood oxygen saturation in the same, deep tissue volume. In particular, we present *in-vivo* rat brain data derived from models of hypercapnia (excess $CO_2$) and hypoxia ($O_2$ deficit); changes in cerebral blood flow, hemoglobin concentration and oxygenation are measured and discussed. This combination of tools has not been previously employed, and because of the increased information it provides about vascular response, we anticipate that the probe will be valuable for future research on the physiology of deep, highly scattering tissue.

## 2 Background on Theory and Instrumentation

A turbid medium such as tissue is characterized by a reduced scattering coefficient $\mu_s'$, and an absorption coefficient $\mu_a$. In general these quantities can depend on position and time. Physically, the reciprocal of $\mu_s'$ is the photon random walk step, corresponding to the length traveled by a photon in the medium before its initial direction becomes randomized; the reciprocal of $\mu_a$ is the absorption length, corresponding to the length scale over which a photon traveling in the medium will be absorbed. For many conditions of practical interest, e.g. in tissues, the photon fluence rate satisfies a diffusion equation [1].

In our experiments light is collected in remission, i.e. light sources and detectors are arranged in a plane parallel to the air/tissue surface, and are oriented to receive or emit light normal to the air/tissue interface. We thus approximate the tissue samples as semi-infinite. The solution for diffuse photon density waves in this geometry is readily obtained using an image source approach [27]. Multidistance measurements of the diffuse photon fluence rate enable one to deduce the optical properties ($\mu_s'$ and $\mu_a$) of the medium by fitting the known analytical solution to the measurements.



In the near-infrared region, the dominant chromophore in tissue is hemoglobin, and the absorption spectra of oxyhemoglobin and deoxyhemoglobin are different [1,28]. Thus, determination of $\mu_a$ at two different optical wavelengths (e.g. 786 nm and 830 nm) provides information sufficient for calculation of the concentrations of oxyhemoglobin and deoxyhemoglobin if one assumes a water/lipids ratio.

We determine the motional dynamics of the medium by measuring the time dependence of detected diffuse light intensity and then computing the (normalized) intensity autocorrelation function. We have recently shown (for continuous light sources) that this autocorrelation function also satisfies a diffusion equation, though the equation differs slightly from that obeyed by the diffuse light fluence rate; in particular there is an additional absorption term that depends on the mean-square displacement of the scatterers (e.g. blood cells) during the autocorrelation time $\tau$ [26,29,30].

Two models can be used to describe the dynamics of cerebral blood flow. The first model was used originally in colloidal suspensions where the dynamics is Brownian [25,31]. The second model argues that in a capillary network, blood flow resembles a random flow, i.e. both the speed and direction of the flow at any point in space are random. In such cases [32,33] the decay rate of the correlation function depends on the mean squared velocity of the scatterers. We have analyzed our data with both models, but parameterize our data using the Brownian diffusion model. Thus the effective blood flow speed is parameterized by the Brownian diffusion coefficient, which is proportional to the exponential decay rate of the measured temporal correlation functions. The relative change of this decay rate equals the relative change of the cerebral blood flow (CBF). Justification and discussion of our assumptions is discussed more fully in [15]. We introduce the term 'diffuse correlation flowmetry' to represent the correlation method described above.

Figure 1 shows a schematic diagram of the instrument. The sources of near-infrared (NIR) light were: (a) a single mode laser source with a coherence length (>1 m) much longer than a typical photon path length, for the diffuse correlation flowmetry measurements and (b) two intensity modulated laser diodes for the diffuse photon density wave measurements. The wavelength of the single-mode laser was tunable from 770 nm to 802 nm (model TC40, SDL Inc., San Jose, CA). The laser diodes operated at 786 nm and 830 nm (manufactured by Sharp and Hitachi respectively). The diffuse photon density wave modulation frequency was 70 MHz. All three lasers were multiplexed into nine optical source fibers in the probe.

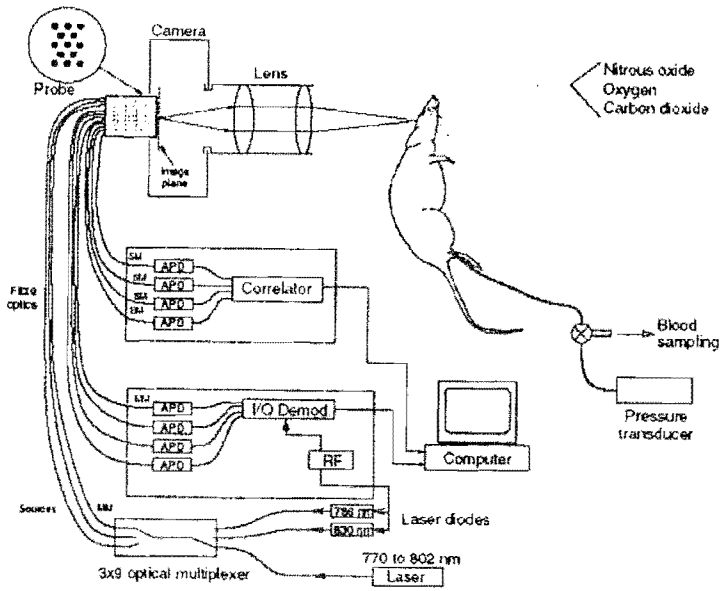


**Figure 1.** A schematic diagram of the experiment. Key: avalanche photodiode (APD), radiofrequency generator (RF), multimode fiber (MM), single-mode fiber (SM), *I/Q* demodulation (I/Q Demod.).

Two sets of four avalanche photodiodes were employed for detection of diffuse light at four positions, one set for the diffuse photon density waves and another set for the diffuse correlation measurement. The amplitudes and phases of the DPDW were measured for each source-detector pair. For diffuse correlation flowmetry, signals from the photodiodes were directed to a correlator chip (Correlator.com, Bridgewater, NJ). The correlator chip computed the temporal intensity autocorrelation functions. A relay lens projecting the probe onto the measuring sample permitted non-contact measurements. The source and detector optical fibers were arranged in a two-dimensional pattern as shown in the upper left corner of the figure. With this design, we could reconstruct low-resolution images of the dynamics and the optical properties from the measurements. The optical multiplexer was controlled remotely by a computer.

Both the DPDW and diffuse correlation measurements take about the same amount of time, and are operated in a time-shared manner with the DPDW measurements



interlaced between successive diffuse correlation measurements. The data presented in this paper were made at about 2.5 min per combined measurement.

## 3 Experimental

Adult male Sprague-Dawley rats weighing 300-325 g were fasted overnight prior to measurements. The animals were anesthetized (Halothane 1-1.5%, $N_2O$ 70%, $O_2$ 30%) and catheters were placed into a femoral artery to monitor the arterial blood pressure and into a femoral vein for drug delivery. The body temperature was maintained at 37±2C. The animal was tracheotomized, mechanically ventilated and fixed on a stereotaxic frame. The probe source-detector plane was placed relay imaged and located symmetrically about midline; it covered a region from 2mm anterior to 6mm posterior of the rhinal fissure. The hypercapnic challenge consisted of elevating blood $p_aCO_2$ by adding carbon dioxide (8%) into the breathing mixture. The hypoxic modulation involved decreasing the arterial $p_aO_2$ by reducing the inspired $O_2$ to 10%.

## 4 Results and Discussion

Figure 2 (*left side*) shows the percent increase from the baseline level of the cerebral blood flow (i.e. the correlation function temporal decay rate) in one experiment where the animal breathed 9% $CO_2$ for 10 minutes. The numbers shown in the figure were averaged over the area of the imaged brain, which comprised an 8x10 $mm^2$ area of cortex. During the $CO_2$ inhalation, the $p_aCO_2$ increased from 38 mmHg to 75 mmHg, and the average relative increase of cerebral blood flow was about 0.77 (77%) from the baseline. Figure 2 also shows the concurrent changes in the hemoglobin concentration and cerebral blood flow as measured by NIR absorption spectroscopy averaged over the same cortical area during hypercapnia. A 0.17 (17%) increase in the hemoglobin concentration was observed. The hemoglobin concentration appears to increase at a slower rate than the cerebral blood flow and also decays slower after the $CO_2$ was switched off. The average relative increase of the hemoglobin oxygenation in the cortex during the same $CO_2$ stimulation is shown in the bottom graph of Figure 2. The increase was about 16%, with the oxygenation dynamics following the flow changes more closely than the total hemoglobin concentration.

We also obtained time courses for hypoxia (not shown). In Figure 2 (*right side*), the relative changes averaged over the last 10 minutes of the hypercapnia are plotted along with the relative changes during hypoxia. The values are obtained averaging the signal from 5 to 15 minutes following the perturbation. For both hypercapnia and hypoxia, vasodilatation increased blood flow (CBF) and blood volume (CBV).

Since oxygen metabolism remains roughly constant during hypercapnia and hypoxia, the flow increases are countered by a reduced oxygen extraction fraction. The measured tissue blood oxygen saturation ($Y_t$) is a combination of arterial, capillary, and venous tissue compartments. During hypercapnia the arterial saturation is constant so that the reduced oxygen extraction fraction results in increased tissue saturation, while during hypoxia, the drop in arterial saturation combined with a decreased oxygen extraction fraction results in decreased tissue saturation. From these two modulations we have measured two different trends in the hemoglobin saturation and blood flow.

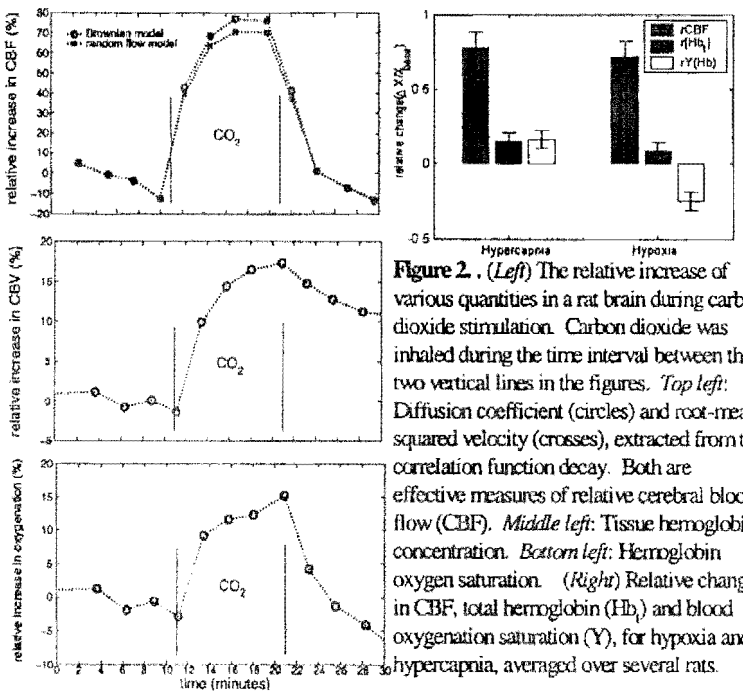


**Figure 2.** (*Left*) The relative increase of various quantities in a rat brain during carbon dioxide stimulation. Carbon dioxide was inhaled during the time interval between the two vertical lines in the figures. *Top left*: Diffusion coefficient (circles) and root-mean-squared velocity (crosses), extracted from the correlation function decay. Both are effective measures of relative cerebral blood flow (CBF). *Middle left*: Tissue hemoglobin concentration. *Bottom left*: Hemoglobin oxygen saturation. (*Right*) Relative changes in CBF, total hemoglobin ($Hb_t$) and blood oxygenation saturation (Y), for hypoxia and hypercapnia, averaged over several rats.



Our combined measurements also offer us the possibility to quantitatively verify that CBF and blood oxygenation changes are self-consistent. We can use a simplified model for oxygen metabolism to relate the two measurements, wherein we assume that the product of the difference in oxyhemoglobin concentration between the artery perfusing the tissue and the vein draining the tissue and blood perfusion rate equals the oxygen consumption rate. The two measurements are consistent within our signal-to-noise. Ultimately this type of analysis will allow us to make low resolution maps of oxygen metabolism, which in turn will provide crucial information about tissue viability and function.

To conclude, we have demonstrated the ability to concurrently measure relative changes in cerebral blood flow, hemoglobin concentration and hemoglobin oxygenation with a single non-contact, non-invasive instrument. Although our pilot measurements are preliminary, results from a rat hypercapnia and hypoxia models are in reasonable agreement with the data taken with other techniques in the literature, and offer the possibility for further growth and quantitation. The optical techniques used in this study are attractive, also, because they enable us to measure the vascular response of deep tissues. We anticipate that the instrument will facilitate other protocols such as hypoxia and hemodilution that affect whole-brain hemodynamics. Finally, the new instrument and concept may be applicable to human studies especially in infants and neonates.

## 5 Acknowledgements

This work is supported by the National Institutes of Health under grant number HL57835-01. We thank B Chance, A Villringer and R Cheung for helpful comments and discussions. Technical assistance from R Choe and L Zubkov is also gratefully acknowledged.

## References

1. Yodh A. G. and Chance B., *Phys. Today* **48** (1995) pp. 34–40.
2. O'Leary M. A., Boas D. A., Chance, B. and Yodh, A. G., *Phys. Rev. Lett.* **69** (1992) pp. 2658–2661.
3. Boas D. A., O'Leary M. A., Chance B. and Yodh, A. G., *Phys. Rev. E* **47** (1993) pp. R2999–3003.
4. Fishkin J. and Gratton E., *J. Opt. Soc. Am. A* **10** (1993) pp. 127–140.
5. Schmitt J. M., Knuttel A. and Knudsen J. R., *J. Opt. Soc. Am. A* **9** (1992) p. 1832.
6. Tromberg B., Svaasand L. O., Tsay T. and Haskell R. C., *Appl. Optics* **32** (1993) pp. 607–616.

7. Walker S. A., Fantini S. and Gratton E., *Appl. Optics.* **36** (1997) pp. 170–179.
8. Schotland J. C., *J. Opt. Soc. Am. A* **14** (1997) pp. 275–279.
9. O'Leary M. A., Boas D. A., Chance B. and Yodh, A. G., *Opt. Lett.* **20** (1995) pp. 426–428.
10. Arridge S. R., *Appl. Optics* **34** (1995) pp. 7395–7409.
11. Arridge S. R. and Schweiger M., *Appl. Optics* **34** (1995) pp. 8026–8037.
12. Yao Y. Q., Wang Y., Pei Y. L., Zhu W. W. and Barbour, R. L., *J. Opt. Soc. Am. A* **14** (1997) pp. 325–342.
13. Jiang H. B., Paulsen K. D., Osterberg U. L. and Patterson M. S., *Appl. Optics* **36** (1997) pp. 52–63.
14. O'Leary M. A., Boas D. A., Li X. D., Chance B. and Yodh A. G., *Opt. Lett.* **21** (1996) pp. 158–160.
15. Cheung C., Culver J. P., Takahashi K., Greenberg J. H. and Yodh A. G., *Phys. Med. Biol.* **46** (2001) pp. 2053–2065.
16. Phelps M. E. and Mazziotta J. C., Positron emission tomography: human brain function and biochemistry. *Science* **228** (1985) pp. 799–809.
17. Kwong K. K. *et al., Proc. Natl Acad. Sci. USA* **89** (1992) pp. 5675–5679.
18. Chance B., *NMR Biomed.* **2** (1989) pp.179–87.
19. Shepherd A. P., and Oberg P. Å., *Laser-Doppler Blood Flowmetry* (Boston: Kluwer) (1990).
20. Villringer A., Them A., Lindauer U., Einhaupl K., and Dirnagl U., *Circ. Res.* **75** (1994) pp. 55–62.
21. Nair P., Whalen W. J., and Buerk D., *Microvasc.Res.* **9** (1975) pp. 158–165.
22. Wilson D. F., Gomi S., Pastuszko A., and Greenberg J. H., *J. Appl. Physiol.* **74** (1993) pp. 580–589.
23. Danen R. M., Wang Y., Li X. D., Thayer W. S., and Yodh A. G., *Photochem. Photobiol.* **67** (1998) pp. 33–40.
24. Maret G., and Wolf P. E., Z. *Phys.* B 65 (1987) pp. 409–413.
25. Pine D. J., Weitz D. A., Chaikin P. M., and Herbolzheimer E., *Phys. Rev. Lett.* **60** (1988) pp. 1134–1137.
26. Boas D. A., Campbell L. E., and Yodh A. G., *Phys. Rev. Lett.* **75** (1995) pp. 1855–1858.
27. Kienle A., and Patterson M. S., *J. Opt. Soc. Am.* A **14** (1997) pp. 246–254.
28. Zijlstra W. G., Buursma A., and Meeuwsen van der Roest W. P., *Clin. Chem.* **37** (1991) pp. 1633–1638
29. Boas D. A., and Yodh A. G., *J. Opt. Soc. Am.* A **14** (1997) pp. 192–215.
30. Hackmeier M., Skipetrov S. E., Maret G., and Maynard R., *J. Opt. Soc. Am.* A **14** (1997) pp. 185–191.
31. Maret G., and Wolf P. E., Z. *Phys.* B 65 (1987) pp. 409–413.
32. Nossal R., Chen S. H., and Lai C. C., *Opt. Commun.* 4 (1971) p. 35.
33. Bonner R., and Nossal R., *Appl. Opt.* **20** (1981) p. 2097.


# SELECTED POSTERS